

Oxygen-vacancy driven electron localization and itinerancy in rutile-based TiO_2

Frank Lechermann,^{1,2} Wolfgang Heckel,² Oleg Kristanovski,¹ and Stefan Müller²

¹*I. Institut für Theoretische Physik, Universität Hamburg, D-20355 Hamburg, Germany*

²*Institut für Keramische Hochleistungswerkstoffe,
Technische Universität Hamburg-Harburg, D-21073 Hamburg, Germany*

Oxygen-deficient TiO_2 in the rutile structure as well as the Ti_3O_5 Magnéli phase is investigated within the charge self-consistent combination of density functional theory (DFT) with dynamical mean-field theory (DMFT). It is shown that an isolated oxygen vacancy (V_O) in titanium dioxide is not sufficient to metallize the system at low temperatures. In a semiconducting phase, an in-gap state is identified at $\varepsilon_\text{IG} \sim -0.75$ eV in excellent agreement with experimental data. Band-like impurity levels, resulting from a threefold V_O -Ti coordination as well as entangled (t_{2g} , e_g) states, become localized due to site-dependent electronic correlations. Charge localization and strong orbital polarization occur in the V_O -near Ti ions, which details can be modified by a variation of the correlated subspace. At higher oxygen vacancy concentration, a correlated metal is stabilized in the Magnéli phase. A V_O -defect rutile structure of identical stoichiometry shows key differences in the orbital-resolved character and the spectral properties. Charge disproportionation is vital in the oxygen-deficient compounds, but obvious metal-insulator transitions driven or sustained by charge order are not identified.

I. INTRODUCTION

From two motivating research directions, the investigation of oxygen-deficient transition-metal oxides has gained enormous renewed interest. First, the emerging field of oxide heterostructures lead to questions concerning the impact of oxygen vacancies on interface properties. Since especially the SrTiO_3 band insulator marks an important heterostructure building block, elucidating the role of such vacancies in that compound has recently attracted lots of attention.^{1–7} Second, on the search of realizing a memristor,⁸ $\text{TiO}_{2-\delta}$ remains a key material.^{9,10} Formation and migration of oxygen-vacancy defects are identified to regulate the resistance modulation therein.

Stoichiometric SrTiO_3 is characterized as a cubic (perovskite) $\text{Ti}^{4+}(3d^0)$ compound with crystal-field split e_g and t_{2g} states (cf. Fig. 1). The band gap is located between the dominantly $\text{O}(2p)$ - and the t_{2g} manifold. Due to the strong $\text{O}(2p) - e_g$ hybridization, the creation of an oxygen vacancy (V_O) leads to local $\text{Ti}^{3+}(3d^1)$ sites and e_g -dominated in-gap states.¹ The interplay of Ti^{4+} - and Ti^{3+} -like states gives rise to a competition between electron localization and itinerancy, posing an intriguing many-body problem. Recently, that problem was approached by theory within the combination of density functional theory (DFT) with dynamical mean-field theory (DMFT).^{5,6,11} Experiments indeed suggest that V_O s on the surface of strontium titanate as well as in the interface of $\text{LaAlO}_3/\text{SrTiO}_3$ may be relevant not only for metallicity, but also for emergent magnetic and/or superconducting order.

Oxygen vacancies in TiO_2 pose a related intricate problem, yet with a twist. Besides single-defect scenarios, long-range-ordered vacancy structures provided by the $\text{Ti}_n\text{O}_{2n-1}$ Magnéli phases^{12–14} are an additional point of materials reference. The role of oxygen vacancies in titanium dioxide, with its twofold structural representations of rutile and anatase is a longstanding problem, and has

so far been studied in several theoretical works based on conventional DFT,¹⁵ using hybrid functionals,^{16–20} as well as by treating static electronic correlations within DFT+U.^{20–24} Within the latter framework, Mattioli *et al.*²¹ originally showed that isolated V_O s in TiO_2 can introduce shallow electronic levels only in anatase, while solely deep localized levels are induced in rutile. The more recent oxygen-deficient rutile studies^{18,22,24} suggest an intricate coexistence of shallow and deep levels.

Electronic structure investigations of various Magnéli phases, which may in fact be derived starting from the rutile structure,¹⁵ furthermore revealed challenging physics, such as e.g. metal-insulator transitions and charge ordering.^{25–27} But those assessments are so far limited by the possibilities of DFT(+U) to describe electron correlation.

In this work we want to provide a theoretical account of electron correlations in oxygen-deficient rutile-based TiO_2 from a DFT+DMFT perspective. This not only provides a relevant examination of defect-mediated electronic self-energy effects beyond Kohn-Sham exchange-correlation treatments for an oxide compound with high potential for technological applications. It also allows

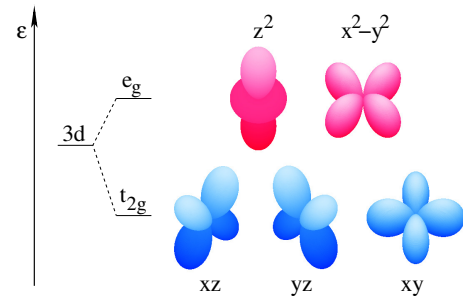


FIG. 1. (color online) Crystal-field splitting of a transition-metal $3d$ shell, located in a full-cubic symmetry environment, into t_{2g} and e_g states.

us to compare the characteristics of the induced defect states to e.g. the ones found in the SrTiO_3 perovskite. We show that energy-similar in-gap states are emerging upon creation of V_{O} s, but metallicity does only occur above a corresponding concentration threshold.

Rutile is known to be the thermodynamically stable TiO_2 phase at all temperatures and pressures,²⁸ while anatase is metastable but can kinetically be stabilised at low temperatures. We therefore restrict the investigation on the rutile structural case of TiO_2 as well as the Ti_3O_5 Magnéli phase as a higher V_{O} -concentration counterpart.

II. COMPUTATIONAL APPROACH

The supercell defect structures of rutile- $\text{TiO}_{2-\delta}$ as well as the Magnéli Ti_3O_5 structure are structurally relaxed¹⁰ on the DFT level within the generalized-gradient approximation (GGA) using the PBEsol²⁹ functional in the VASP code.^{30–33}

Our present charge self-consistent DFT+DMFT framework^{34–36} builds up on the mixed-basis pseudopotential approach^{37,38} for the DFT part and the continuous-time quantum-Monte-Carlo method^{39,40}, as implemented in the TRIQS package,^{41,42} for the DMFT impurity problem. We utilize the GGA in the PBE⁴³ functional form within the Kohn-Sham cycle.

Locally, threefold effective $\text{Ti}(3d)$ functions define the correlated subspace, which as a whole consists of the corresponding sum over the various Ti sites in the defect problem. Projected-local orbitals^{44–48} of $3d$ character provide the effective functions from acting on Kohn-Sham conduction states above the $\text{O}(2p)$ -dominated band manifold. Note that the resulting effective orbitals are not of exclusive t_{2g} - or e_g kind, but are defined by the local three-orbital sector lowest in energy, respectively. Each Ti site marks an impurity problem, and the whole number of explicitly treated impurity problems depends on the number of symmetry-inequivalent transition-metal sites in the given supercell. A three-orbital Hubbard Hamiltonian of Slater-Kanamori form, if not otherwise stated parametrized by the Hubbard $U = 5 \text{ eV}$ and the Hund's exchange $J_{\text{H}} = 0.7 \text{ eV}$, is active on each Ti site. These values for the local Coulomb interactions are in line with previous studies on titanates.^{49–52} A double-counting correction of the fully-localized form⁵³ is utilized in this work. The analytical continuation of the finite-temperature Green's functions on the Matsubara axis $i\omega$ to real frequencies is performed via the maximum-entropy method.

Note that we study only paramagnetic states without broken spin symmetry, as well as charge-neutral lattice configurations. Yet possible inter-site charge disproportionation is surely allowed.

III. RESULTS

A. Rutile TiO_2

To set the stage for the discussion of oxygen-deficient titanium dioxide, we briefly discuss the electronic structure at stoichiometry. The rutile structure⁵⁴ (see Fig. 2a) has tetragonal symmetry (space group $P4_2/mnm$) with a ratio $c/a = 0.64$ and the primitive cell comprises two TiO_2 formula units. It consists of corner- and edge-sharing TiO_6 octahedra, such that each oxygen ion is coordinated by three neighboring titanium ions. This is in contrast to common perovskite-based titanates, where the TiO_6 octahedra are exclusively corner-sharing and O is twofold Ti-coordinated. Of the three rutile minimal Ti-O bond lengths, the two shorter ones are identical in extent. Nominally, titanium is in the Ti^{4+} oxidation state with $3d^0$ occupation.

The given compound is a band insulator with an experimental (optical) band gap of size $\Delta_{\text{g}} \sim 3 \text{ eV}$.^{55–57} Conventional DFT calculations yield a smaller gap $\Delta_{\text{g}} \sim 2 \text{ eV}$ (cf. Fig. 2b). Since TiO_2 is a nominal $3d^0$ material, the HOMO orbitals are of dominant $\text{O}(2p)$ kind and the LUMO orbitals are mainly of $\text{Ti}(3d_{t_{2g}})$ character, while dominant $\text{Ti}(3d_{e_g})$ is located at even higher energies above the band gap. Because of the fact that the c -axis and the main TiO_6 -octahedra axes are locally

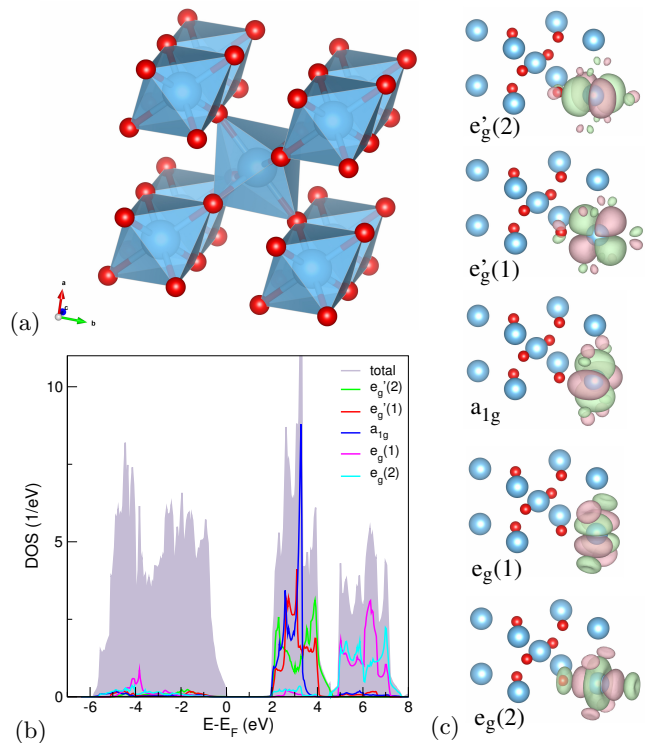


FIG. 2. (color online) Characterization of rutile- TiO_2 . (a) Crystal structure with Ti (large blue/grey) and O (small red/dark) atoms. (b) Total and local-orbital GGA density of states. (c) Projected local $\text{Ti}(3d)$ orbitals.

orbital	ε_{CF}	$ z^2\rangle$	$ xz\rangle$	$ yz\rangle$	$ x^2 - y^2\rangle$	$ xy\rangle$
$ e'_g(2)\rangle$	2684	0.000	0.000	0.000	1.000	0.000
$ e'_g(1)\rangle$	2653	0.000	0.707	0.707	0.000	0.000
$ a_{1g}\rangle$	2574	-0.827	0.000	0.000	0.000	-0.562
$ e_g(1)\rangle$	4398	0.000	-0.707	0.707	0.000	0.000
$ e_g(2)\rangle$	4413	0.562	0.000	0.000	0.000	-0.827

TABLE I. The titanium $t_{2g} = (e'_g(2), e'_g(1), a_{1g})$ and $e_g = (e_g(1), e_g(2))$ orbitals in TiO_2 with their respective crystal-field level ε_{CF} (in meV), expressed in terms of cubic harmonics.

aligned trigonal, the $\text{Ti}(t_{2g}, e_g)$ orbitals may be written as linear combinations of cubic harmonics from diagonalization of the orbital-density matrix (see Tab. I). Due to the local symmetry, the internal (t_{2g}, e_g) degeneracies known from the full octahedral group are lifted, respectively. Comparison of the crystal-field levels ε_{CF} marks the a_{1g} level as the lowest one, 110 meV below $e'_g(2)$. The t_{2g} -based states are about 2.2 eV lower in energy than the e_g -based ones. Within the effective t_{2g} manifold, which has a bandwidth of about 2.5 eV, the $e'_g(2)$ orbital is designated since its lobes point along the in-plane tetragonal axes (see Fig. 2c).

B. Oxygen vacancy in rutile TiO_2

1. Structural details and correlated subspaces

As shown in Fig. 3, a supercell five times the size of the primitive cell, i.e. with 10 Ti and 20 O atoms, serves as basis structure for the defect study. A single V_O leaves three nearest-neighbor titanium ions behind, here labelled Ti1, Ti2 and Ti3. In the stoichiometric rutile structure, the Ti2-Ti3 distance marks the short side of the given Ti triangle. The nominal V_O concentration in this constellation amounts to $c \equiv \delta/2 = 0.05$, i.e. our modeling describes a $\text{TiO}_{1.9}$ defect case. This represents a large V_O concentration, however not unrealistic for the given system.⁵⁸ Table II shows that the inter-atomic distances are only weakly modified upon structural relaxation, which may be also related to the small supercell size. Still, the obtained pattern describes a shortening of the Ti1-Ti2,3 distances and an elongation of the Ti2-Ti3 bonding, providing a trend to balance the triangle distances through the V_O .

In the following we want to investigate the effect of an V_O in the rutile structure in terms of the local-orbital configuration as well as the net electronic structure. We will discuss two different choices for the correlated subspace. First in section III B 2, that space is formed by *all* Ti sites in the given structure, which marks the canonical and ground-state-oriented case. Second in section III B 3, the correlated subspace is *restricted* to the contribution of the Ti1-3 sites, i.e. it becomes more local. This second

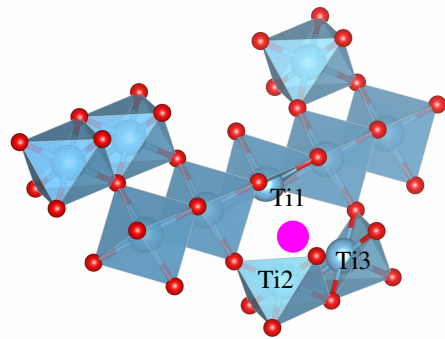


FIG. 3. (color online) Structural characterization of an oxygen vacancy (large purple/lightgrey) in rutile.

	Ti1–Ti2	Ti1–Ti3	Ti2–Ti3
TiO_2	3.57	3.57	2.96
$\text{TiO}_{1.9}$	3.53	3.53	2.97

TABLE II. Comparison of the inter-atomic distances (in Å) between Ti ions surrounding a vacancy-designated oxygen site.

choice may be interpreted as treating an excited state of the system, where electrons do not see the explicit Coulomb repulsion on the remaining Ti sites. Since the $3d$ occupation on the original $\text{Ti}(d^0)$ sites distant to the V_O is expected small, double occupation is there rather rare. If moreover the electrons have gained energy from an excitation process, they can even more easily escape from such double occupations (as well as more efficiently screen the Coulomb penalties). Thus the average effect of local U and J_H on the V_O -distant Ti sites can then be neglected to a good approximation to obtain a rough picture of the present system on a *globally-higher* excitation level. This approximation and interpretation is also not in conflict with the definition of a one-particle spectral function. We thus simply term that space 'excited correlated subspace', and this second choice allows us to shed light on possible changes in the oxidation state of the oxygen vacancy. Still note however that the Coulomb interactions on the Ti sites away from the V_O s are crucial to understand the semiconducting character of $\text{TiO}_{2-\delta}$, as will be explained in the following section III B 2.

2. Canonical correlated subspace formed by all Ti sites

Let us start with the well-defined DFT+DMFT setting of the correlated subspace build by all the Ti sites. On the GGA level, as displayed by plotting the total spectral function $A(\omega) = \sum_{\mathbf{k}} A(\mathbf{k}, \omega)$ in Fig. 4, the considered system becomes metallic with semimetallic tendencies around the Fermi level ε_F positioned within the t_{2g} manifold. Yet correlations and finite temperature T render the situation more intriguing. At low T the

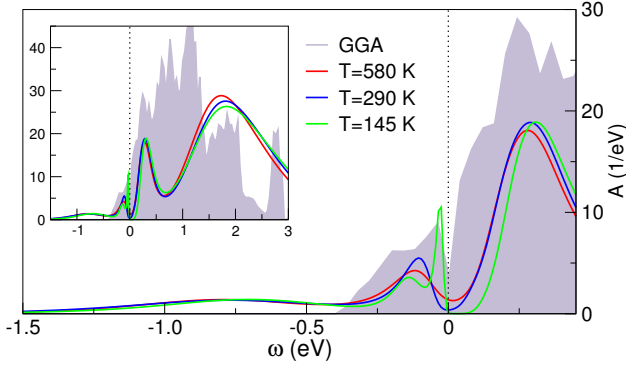


FIG. 4. (color online) Total spectral information for rutile-TiO_{1.9} in GGA and DFT+DMFT, at different temperatures in two energy windows.

defect structure is semiconducting within DFT+DMFT, with a small charge gap $\Delta \sim 0.06$ eV at $T = 145$ K. That gap is filled with rising temperature, marking a bad-metal regime. In addition, there is sizable transfer of spectral weight to a broad in-gap structure centered at $\varepsilon_{IG} \sim -0.75$ eV. Note that optics measurements detect an absorption peak in reduced semiconducting TiO₂ single crystals at 0.75 eV,^{55,56} commonly used to explain its blue color.⁵⁸ Photoemission measurements on the rutile surface report a defect-state peak at ~ -0.9 eV,^{59–61} while on the anatase surface it is located at an higher energy of ~ -1.1 eV^{59,62} Furthermore, scanning tunneling spectroscopy finds an in-gap state at ~ -0.7 eV on the defect-rutile surface⁶³ and x-ray photoelectron spectroscopy on rutile TiO₂ nanoparticles reveals a defect state at ~ -0.8 eV.²⁰ It is tempting to relate these experimental findings of deep levels in TiO_{2- δ} to the present satellite peak. On the other hand, n -type conductivity with rather high mobilities due to shallow level has been also reported in the literature,⁶⁴ which might be connected to our small-gap feature.

To gain insight in the nature and characteristics of the Ti-local states near the V_O, first Tab. III provides the effective orbitals on Ti1-3 written in terms of linear combinations of the original (t_{2g}, e_g) functions from Tab. I. The φ and φ' orbitals on Ti2,3 behave very similarly, therefore we restrict the discussion to the φ branch. It is seen that while the ψ_2 orbital has strong e_g character, the orbitals φ_1, φ_2 have sizable contributions from both original orbital sectors. Thereby φ_1 is t_{2g} -dominated and φ_2 is e_g -dominated. Thus a nearly exclusive e_g character of the local defect states, as e.g. given in oxygen-deficient SrTiO₃,^{1,6} does not apply for oxygen vacancies in TiO₂. Note furthermore that the $e'_g(2)$ orbital has almost negligible contribution to the V_O-induced physics, as the $e'_g(2)$ -dominated φ_3 orbital remains nearly empty.

Concerning tight-binding parameters, the hopping between both φ_1 on Ti2 and Ti3 is largest with $t_{\varphi_1} = -0.2$ eV, while the other hopping amplitudes on the Ti triangle are of absolute value ≤ 0.1 eV. Non-surprisingly, this marks Ti2,3 as more strongly coupled, thus possibly

site	orbital	ε_{CF}	$ e'_g(2)\rangle$	$ e'_g(1)\rangle$	$ a_{1g}\rangle$	$ e_g(1)\rangle$	$ e_g(2)\rangle$
Ti1	$ \psi_1\rangle$	1102	0.035	-0.999	0.000	0.000	-0.002
	$ \psi_2\rangle$	698	0.000	0.000	-0.147	-0.006	0.990
	$ \psi_3\rangle$	1023	0.000	0.001	0.990	-0.003	0.147
Ti2	$ \varphi_1\rangle$	710	-0.032	-0.023	0.837	-0.427	-0.214
	$ \varphi_2\rangle$	785	0.077	0.073	0.308	0.733	0.473
	$ \varphi_3\rangle$	992	-0.759	-0.642	-0.221	0.096	0.058
Ti3	$ \varphi'_1\rangle$	709	0.036	-0.027	0.872	0.437	-0.220
	$ \varphi'_2\rangle$	780	0.083	-0.079	-0.488	0.726	-0.470
	$ \varphi'_3\rangle$	992	0.758	-0.641	0.018	-0.103	0.063

TABLE III. Effective V_O-induced orbitals on the three nearby Ti sites in the rutile structure, with their respective crystal-field level ε_{CF} (in meV), written in terms of linear combinations of the original (t_{2g}, e_g) functions.

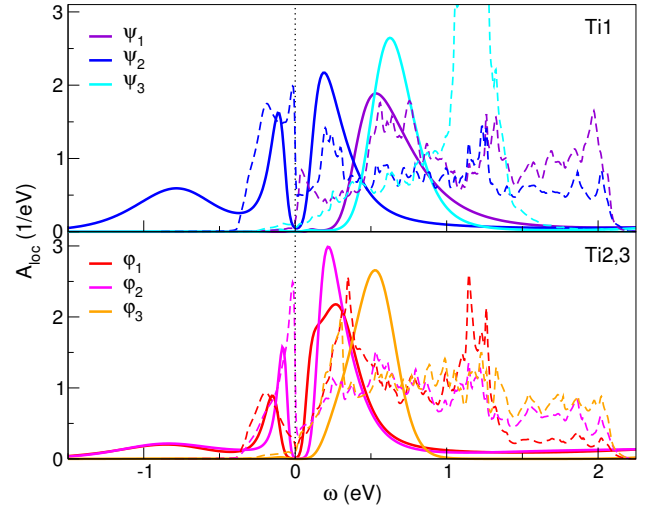


FIG. 5. (color online) Local spectral information for rutile-TiO_{1.9} on Ti1 and Ti2,3 (cf. Fig. 3) at $T = 290$ K. Dashed lines correspond to the GGA result, respectively.

prone to singlet/triplet formation.

Figure 5 provides the spectra on Ti1-3, which are expected to display (partly) Ti³⁺ character. Note that although all Ti sites in the supercell contribute to the full correlated subspace, electron occupation on the remaining Ti sites is very small. The filling on the Ti sites farther away from V_O is also not significantly raised with temperature. The effective orbitals on Ti2 and Ti3 are nearly equivalent by symmetry and behave here very similarly, so no site differentiation is needed. Of the three correlated orbitals $\{\psi_m\}$ on Ti1, only ψ_2 has sizable filling. Spurious occupation of ψ_1, ψ_3 in GGA is eliminated by correlations. On the contrary, two orbitals, i.e. φ_1 and φ_2 are occupied on Ti2,3. The designation of ψ_2, φ_1 and φ_2 is already suggested from their favorable crystal-field levels (cf. Tab. III). In DFT+DMFT the occupations read $(n_{\psi_2}, n_{\varphi_1}, n_{\varphi_2}) = (0.65, 0.29, 0.33)$,

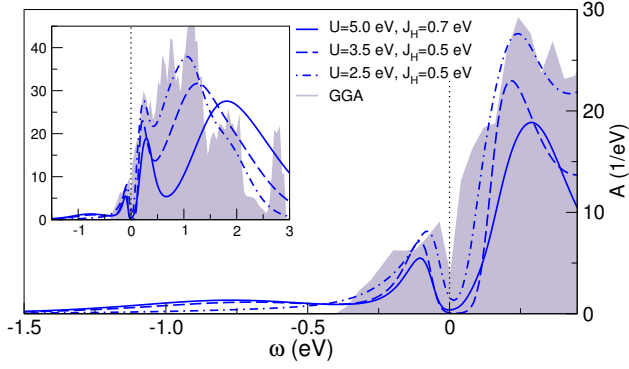


FIG. 6. (color online) Total spectral function for rutile $\text{TiO}_{1.9}$ based on three different sets of local Coulomb interactions at $T = 290$ K.

thus all three Ti sites have similar occupation, however $n_{\text{Ti1}} > n_{\text{Ti2,3}}$ holds. Since the site-resolved fillings sum up to $n_{V_O} = 1.89$ and oxygen is in the O^{2-} oxidation state in the compound, the defect is described as of being close to the nominal neutral vacancy state V_O^0 .

In order to check for the influence of the chosen local Coulomb interactions on the physics, we additionally performed calculations for $U = 3.5$ eV and $U = 2.5$ eV, both with $J_H = 0.5$ eV. The values $U = 3.5$ eV, $J_H = 0.5$ eV were used in a recent DFT+DMFT study of the oxygen-deficient SrTiO_3 surface.⁶ There are no qualitative differences between the resulting total spectral functions (cf. Fig. 6) for the sets ($U = 5$ eV, $J_H = 0.7$ eV) and ($U = 3.5$ eV, $J_H = 0.5$ eV), hence the detected physics is rather stable within a reasonable range of local Coulomb-interaction parameters. Only at much smaller $U = 2.5$ eV the semiconducting gap as well as the deeper in-gap state seem to disappear.

It remains to specify the likely mechanism behind the DFT+DMFT finding. The results suggest that the V_O provides electron doping by initially forming rather shallow states below the original t_{2g} manifold. Because of the higher O-Ti connectivity and the entangled (e_g, t_{2g}) defect signature in rutile, both compared to e.g. surface SrTiO_3 ,⁶ the coherency of those states is increased and they seemingly develop band-like character. Sizable Coulomb interactions then lead to a Mott criticality, resulting in band renormalization and formation of Hubbard(-like) bands. The latter give rise to the deep-level in-gap spectra. Importantly, the driving force between the Mott(-like) gap formation is different from a conventional correlated multi-band lattice problem. Since the local states near the V_O are connected *between* different V_O s by fragile hopping paths, mainly the local Coulomb interactions on the Ti sites *distant* from the defects are determinative for driving the doped system again insulating. In other words, the 'interstitial' Coulomb-repulsive region between the V_O s destroys the fragile band-like defect states and localizes the electrons dominantly near the oxygen vacancy.

3. Excited correlated subspace formed by Ti1, Ti2, Ti3

Letting only the sites Ti1-3 contribute to the correlated subspace serves to goals. First, it gives access to a possibly different V_O charging state. Second, it provides a check for our presented mechanism, denoting the Coulomb interactions on Ti away from V_O as being mainly to be blamed for the semiconducting character.

In general, the states V_O^0 , V_O^{+1} and V_O^{+2} are discussed for oxygen-deficient TiO_2 ,^{18,22,24,65} which in other works appeared relevant to fit findings of shallow-donor properties and well-localized defect states within a coherent picture. As discussed in section IIIB 2, the present DFT+DMFT study already provides means to such a co-existence by revealing small-gap as well as deeper in-gap features. Nonetheless, by performing additional calculations within the local-restricted correlated subspace one may learn further details of the V_O energy-level structure. Note that in principle the local Coulomb interactions also change when the correlated subspace is modified, i.e. in the present scenario should be lowered for the smaller subspace. But for simplicity we keep $U = 5$ eV

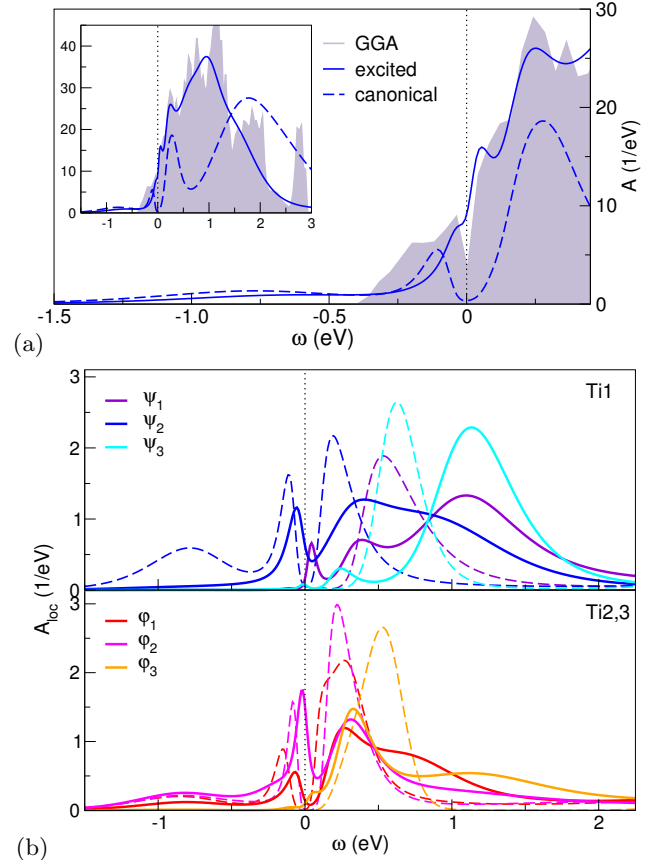


FIG. 7. (color online) Comparison of spectral information for rutile- $\text{TiO}_{1.9}$ using the canonical and the excited correlated subspace at $T = 290$ K. (a) Total spectral function. (b) Local spectra for Ti1 and Ti2,3 (cf. Fig. 3) at $T = 290$ K, full lines: excited, dashed lines: canonical.

and $J_H = 0.7\text{ eV}$ on Ti1-3 to reveal the key features of the excited system.

As expected, a metallic solution results from the calculation, with reduced and shifted incoherent weight at higher energy (see Fig. 7a). This is indeed in favor of our 'interstitial Coulomb' mechanism being relevant for fully localizing electrons near V_O s. Interestingly, the Ti1-3 sites now display a rather different local filling in the dominant orbitals, namely $(n_{\psi_2}, n_{\varphi_1}, n_{\varphi_2}) = (0.24, 0.19, 0.43)$, and a total filling of these sites amounting to $n_{V_O} = 1.56$. This means that in the excited scheme not only the total filling of Ti close to V_O is substantially reduced compared to the canonical scheme, but also the local filling symmetry is different. Now the Ti2,3 sites are majorly occupied and the Ti1 site plays the weaker role, also visualized by plotting the local spectral functions in Fig. 7b. The high-energy, incoherent and strongly-localized part of the spectra is now dominantly carried by states on Ti2,3. It appears that in the excited-system calculation, localized charge on Ti1 has been partially transferred to itinerant states.

These findings are indeed reminiscent of the identification of different V_O charging states in DFT+U and/or DFT hybrid-functional studies.^{18,22,24} Also the characterization of two different site-orbital levels has been reported before, yet usually by invoking explicit magnetic ordering. Our two detected charging states with $n_{V_O}^{\text{can}} = 1.89$, reading $V_O^{+0.11}$, and $n_{V_O}^{\text{ex}} = 1.56$, reading $V_O^{+0.44}$, do not very strongly deviate from the neutral-vacancy case. However note that highly-oxidized states like V_O^{+1}/V_O^{+2} are usually found in the presence of additional trivalent substitutional impurities on the Ti site, such as Fe^{3+} and Cr^{3+} .⁶⁵ An established theoretical picture¹⁸ describes the vacancy-defect state as a bound object consisting of V_O^{2+} plus two polarons, rendering it charge neutral again. In principle one may try to interpret our results also along such lines, since the present filling scenario with Hubbard-like high-energy spectral parts point to a local $S = 1$ spin in the paramagnetic material. On the other hand, as discussed, we do not *have to* invoke the polaron picture on clear grounds to account for the coexistence of shallow and deep states.

Let us finally note that the overall qualitative picture that we here derived for a single V_O in rutile TiO_2 is believed to be stable against modified structural relaxations, as e.g. provided by a different(larger) supercell. More dilute V_O cases could still lead to a weakening of the shallow levels in favor of the deep level, with an increase of the semiconducting gap. Within the local-level manifold the subtle details of the energy hierarchy might be affected by structural issues. But the general notion of the relevant ψ_2 on Ti1 as well as φ_1 and φ_2 on Ti2,3 appears robust.

C. Higher oxygen-vacancy concentration: Ti_3O_5

1. Spectral properties and total energies

We now shift attention to the problem of oxygen vacancies at higher concentration. In order to gain insight in the properties of V_O s in a designated ordered limit, we study a specific Magnéli compound at Ti_3O_5 stoichiometry. There is strong interest in the various Magnéli phases at Ti_3O_5 ,^{12,26,27,66–68} since e.g. photoreversible phase transitions occur at room temperature. But as we are interested in the main effect of vacancy ordering, we focus on a single allotrop, the so-called γ phase. The underlying crystal structure has monoclinic symmetry and can be stabilized at room temperature.⁶⁶

Described in simple terms, whereas perovskite SrTiO_3 has corner-sharing TiO_6 octhedra and rutile TiO_2 an elementary alternation of corner- and face-sharing octhedra, the Magnéli phases exhibit more complicated arrangement of those two octahedra-sharing types to accommodate a desired stoichiometry (see Fig. 8a). This may be interpreted as an ordering of vacancies, however importantly, contrary to e.g. our $\text{TiO}_{1.9}$ structure, there is no V_O -induced 'destruction' of local TiO_6 octhedra. In terms of a formal oxygen deficiency δ , the given Ti_3O_5

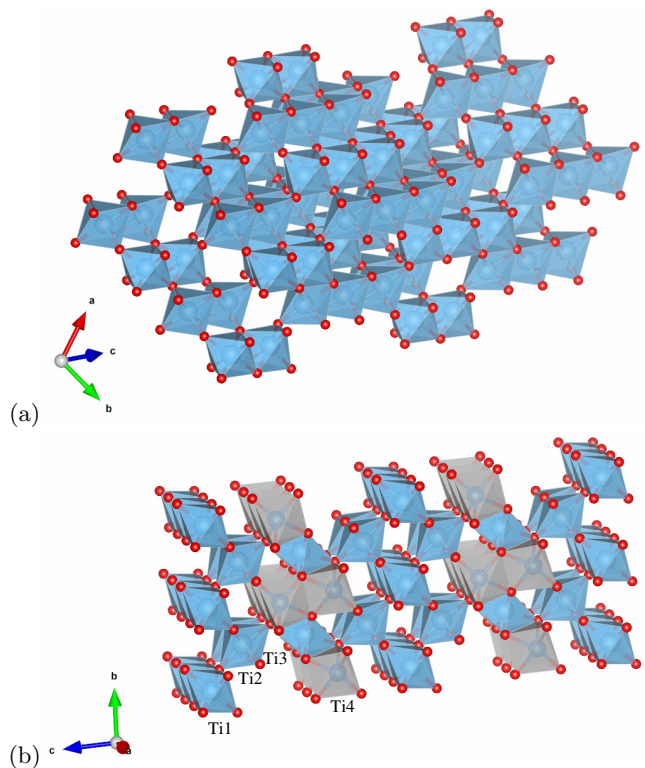


FIG. 8. (color online) Illustration of (a) the γ - Ti_3O_5 structure and (b) the defect-rutile Ti_3O_5 structure, both with Ti (large blue/grey) and O (small red/dark) atoms. In (b), the labels Ti1-4 mark symmetry-inequivalent Ti sites, with grey polyhedra surrounding the 5-fold coordinated Ti4 sites.

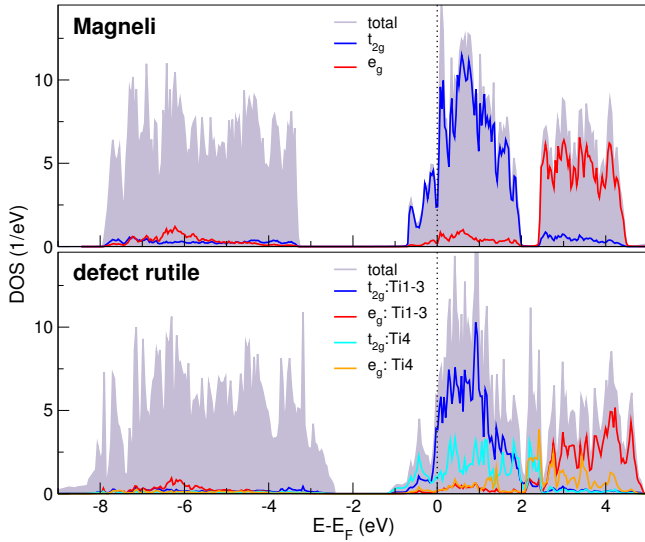


FIG. 9. (color online) Comparison of the GGA density of states of γ -Ti₃O₅ (top) and defect-rutile Ti₃O₅ (bottom), in view of (t_{2g} , e_g) contributions. The labeling Ti1-3 and Ti4 refers to the sites marked in Fig. 8b.

stoichiometry amounts nonetheless to $\delta = 0.33$, i.e. the compound would correspond to TiO_{1.67} with vacancy concentration $c = 0.167$.

In order to compare the electronic characteristics of the optimal-ordered Magnéli structure with V_Os in rutile, we in addition performed calculations for defect rutile with stoichiometry Ti₃O₅. The corresponding crystal structure (cf. Fig. 8b) was determined by energy minimization of oxygen-vacancy arrangements at the desired composition by making use of the cluster-expansion technique (see Ref. 10 for details). In this defect-rutile structure, part of the TiO₆ are indeed ‘damaged’, resulting in selected fivefold-O coordinated Ti sites, here designated as Ti4. A total-energy comparison on the GGA level, as expected, clearly favors the Magnéli structure. The more clever restoration of ideal 6-fold-oxygen coordination around Ti is appreciated by a substantial ~ 0.42 eV per Ti atom against defect rutile.

Figure 9 documents the differences in the GGA density of states in terms of the partitioning in Ti(t_{2g} , e_g)-like contributions. Based on the robust TiO₆-octahedral structuring of the Magnéli phase, the electronic structure of γ -Ti₃O₅ shows a clear distinction into those $3d$ submanifolds. This is partly also true for defect-rutile Ti₃O₅, yet the (t_{2g} , e_g) states from the TiO₅ polyhedra show there more substantial overlap in energy. In fact, the small t_{2g} - e_g gap region above 2 eV in γ -Ti₃O₅ just becomes filled by such states in the defect-rutile structure.

The total spectral functions obtained within DFT+DMFT are plotted in Fig. 10. Both systems remain metallic with including many-body correlations. A lower Hubbard band located at ~ -1.1 eV and renormalization at low energy are identified for the Magnéli

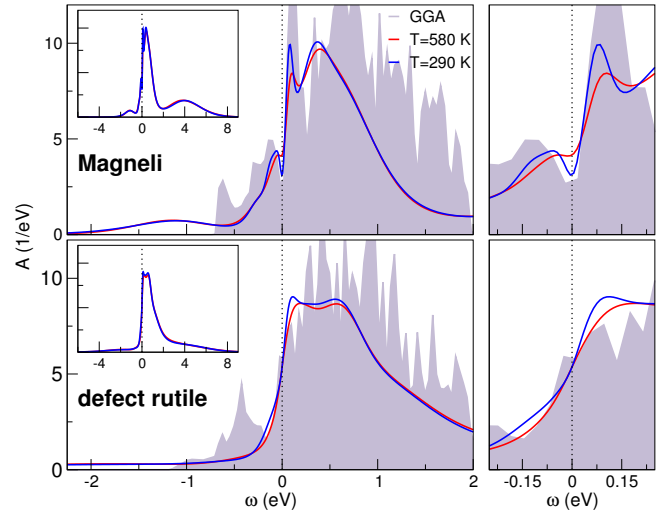


FIG. 10. (color online) Comparison of the correlated total spectral function of γ -Ti₃O₅ (top) and defect-rutile Ti₃O₅ (bottom) at two different temperatures.

phase. This marks the system as a seemingly ‘textbook’ correlated material, with coherent renormalized quasi-particles at low energy and incoherent Hubbard bands at higher energies. Already on the GGA level there is a small spectral dip at the Fermi level, verified also with correlations at lower temperature. Note that the Hubbard band is of course nearly exclusively formed by t_{2g} -like states. Satellite structures of t_{2g} kind have recently been detected in a hard x-ray photoelectron spectroscopy study of the structurally different β -Ti₃O₅ and λ -Ti₃O₅ Magnéli compounds.⁶⁹

Though the same total filling scenario holds for the defect-rutile phase, the characterization with electronic correlations appears more subtle. First, in view of the semiconducting defect-rutile state discussed in section IIIB2, the metallic response at higher V_O concentration is not that surprising. The fragile hopping paths between V_O-near electronic states become increasingly robust with growing concentration of vacancies, such that eventually Coulomb repulsion is not anymore capable of establishing a charge-gapped material. In the low-energy spectrum there is some renormalization due to correlations, but not of significant kind. On a first glance, the spectral function looks furthermore rather monotonic in the occupied part, yet importantly, not necessarily implying that correlations are weak. Because the comparison to the GGA results shows, there is significant spectral-weight transfer to energies far away from the Fermi level, too. However this transfer does not give rise to an obvious lower Hubbard-band peak, but is broadly distributed over a wider energy range (see inset of Fig. 10). This finding is somewhat reminiscent of observations made in resonant-photoemission experiments on electron-doped SrTiO₃.⁷⁰ There, broader in-gap weight was assigned to the increased relevance of Ti($3d$)-O($2p$) hybridization. Since the e_g character, which is more strongly hybridized

with $O(2p)$ than t_{2g} , plays a more prominent role in the defect-rutile case, the present result could possibly point to a similar interpretation. On the other hand, a recent GW+DMFT study suggests the possibility of diminished satellite peaks in some correlated compounds, as well as a reinterpretation of their original character.⁷¹

The total-energy difference between both Ti_3O_5 structural types is even slightly increasing with including many-body correlations. At room temperature, the Magnéli phase is favored by ~ 0.46 eV per Ti atom.

2. Charge disproportionation between Ti sites

So far we did not comment on the local occupations of the respective Ti sites in γ - and defect-rutile Ti_3O_5 . Since the nominal oxidation state at that stoichiometry amounts to $Ti^{3.33+}$, charge fluctuations are expected to be more relevant than in many other oxides with nominal integer Ti valence. In fact, charge ordering in connection with a metal-insulator transition is commonly discussed for various Magnéli phases, especially for the Ti_4O_7 compound.²⁵

The oxygen deficiency quite naturally introduces symmetry-inequivalent Ti sites with potentially different electron occupation. Figure 8b shows four different Ti sites with especially the Ti4 site surrounded only by five oxygen atoms. The γ - Ti_3O_5 structure formally has eight Ti sites different by symmetry, which were also differently treated in our calculations. In the discussion however, to a very good approximation, four Ti classes may be grouped to a single effective class, respectively, since the local-orbital structure only marginally differs. Figure 11 displays the present Magnéli structure in that effective two-Ti-sublattice picturing. An obvious pattern is derived therefrom. The TiO_6 octahedra of Ti sites within a given sublattice are corner sharing, whereas the octahedra are edge sharing between both sublattices. Therefore the intra-sublattice Ti-Ti distance is about 0.5 \AA longer than the inter-sublattice pair distance. Both effective sublattices are not of equal-site size, since the Ti2 sublattice (dark-blue octahedra in Fig. 11) covers twice as many Ti sites as the Ti1 sublattice (light-blue octahedra in Fig. 11). Note that the Ti1 octahedra mark the middle of the stoichiometric undisturbed TiO_2 rutile slabs, which consist of three octahedra in the rutile (001) direction and are interrupted by a (121) V_O defect plane.

Tables IV and V provide the $Ti(3d)$ occupations for both considered Ti_3O_5 structures. Nonsurprisingly in defect rutile, the charge on the Ti4 sites with 5-fold oxygen coordination is largest, marking that site with a $Ti^{2.8+}$ oxidation state. The nearby Ti3 sites are still close to Ti^{3+} , while Ti1-2 are closer to Ti^{4+} . There are no dramatic differences between the numbers based on GGA and those from DFT+DMFT, only the occupation of Ti4 is still somewhat higher with correlations.

The Magnéli phase γ - Ti_3O_5 has a more subtle Ti ordering. The geometrical constraints of keeping the TiO_6

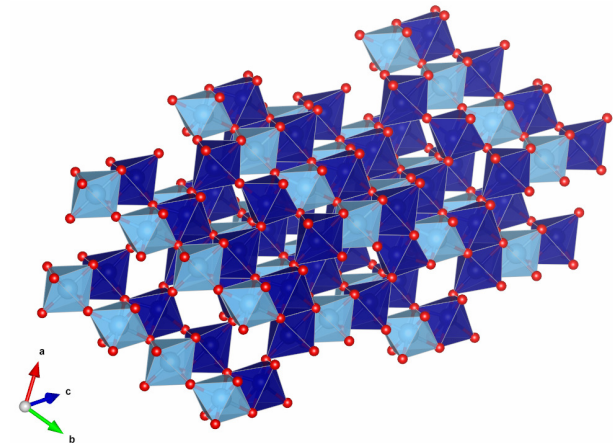


FIG. 11. (color online) Effective two-Ti-sublattice representation of γ - Ti_3O_5 (see text). Light(Dark) blue octahedra correspond to Ti sites on sublattice 1(2).

	GGA	DFT+DMFT($U = 5 \text{ eV}$)
Ti1	0.22	0.20
Ti2	0.26	0.24
Ti3	0.90	0.86
Ti4	1.15	1.23

TABLE IV. Comparison of the $3d$ filling of the different Ti sites in defect-rutile Ti_3O_5 (see Fig. 8b for Ti labeling). The DFT+DMFT data is taken at $T = 290 \text{ K}$.

	GGA	DFT+DMFT	
		$U = 5 \text{ eV}$	$U = 8 \text{ eV}$
Ti1	0.740	0.752	0.766
Ti2	0.630	0.624	0.617

TABLE V. Comparison of the $3d$ filling on the two effective sublattices in γ - Ti_3O_5 (see Fig. 11 for Ti-sublattice labeling). The DFT+DMFT data is taken at $T = 290 \text{ K}$.

octahedra in line with the nominal $Ti^{3.33+}$ state leads to slightly different charge states on both effective sublattices. The smaller Ti1 sublattice carries already on the GGA level more charge, with a disproportionation $\rho(Ti1) - \rho(Ti2) = 0.11 e^-$. Electronic correlations increase this charge splitting only by small amounts, even when invoking a rather large Hubbard $U = 8 \text{ eV}$. Importantly, the system remains always metallic. Also because a seemingly straightforward Ti^{3+}/Ti^{4+} splitting, as in principle possible in the Ti_4O_7 Magnéli system with a nominal $Ti^{3.5+}$ oxidation state, is not an obvious option. Note however that there is also a metal-insulator transition reported for Magnéli Ti_3O_5 ,²⁷ but from γ - Ti_3O_5 to δ - Ti_3O_5 upon lowering temperature. Thus further structural changes are in addition indispensable to allow for insulating behavior.

D. Summary and discussion

We presented a detailed first-principles many-body investigation of the effect of oxygen vacancies in rutile TiO_2 , both in the lower- and the higher-concentration regime. In the former case, the DFT+DMFT results directly provide the three key ingredients known from experiment for $\text{TiO}_{2-\delta}$, namely semiconducting behavior, shallow levels as well as deep levels. Our deep-level (or in-gap) positioning is in excellent agreement with results from various experimental studies. Thereby the many-body perspective provides a different viewpoint on the longstanding discussion of deep vs. shallow levels for oxygen-deficient TiO_2 . Here, both levels are connected in the many-body sense, similar as a lower Hubbard band and a renormalized quasiparticle state in a conventional moderately correlated metal. Still the correlation-induced gap opening in the band-like initial shallow levels is not of standard Mott type. Key to the electron localization at low V_O concentration is the Coulomb-repulsion region between defects, that blocks the fragile hopping paths. Therefore, the resulting charge gap is rather small and does not scale with U in a conventional way.

By invoking an excited correlated subspace we brought the semiconducting solution into the transport regime, therewith showing that indeed the Coulomb interactions on the Ti sites distant from the oxygen vacancies dominantly control the competition between itinerancy and localization. Moreover, the localized states at the V_O display a different occupation and energy state upon excitation. This connects our study to other (static-correlation) theory work for $\text{TiO}_{2-\delta}$, where e.g. different V_O charge states and polaron formation are discussed.^{16–24}

In comparison to oxygen-deficient SrTiO_3 , the defect-rutile problem differs in two crucial points. First, the defect structure with a V_O in nearest-neighbor distance to *three* Ti sites, contrary to *two* Ti sites in the perovskite structure, fosters a modified oxygen-vacancy impact. The higher connectivity with the defect gives way to the formation of more band-like impurity states on the single-electron level. Second, the higher entanglement between t_{2g} and e_g states lifts the electron dichotomy observed on the $\text{SrTiO}_{3-\delta}$ surface,⁶ suppressing both, a decoupled t_{2g} band formation and a rather disconnect straightforward e_g deep-level formation. Therefore at small V_O concentrations, rutile TiO_2 remains insulating (or semiconducting) due to correlation-induced gap opening in (t_{2g}, e_g) -entangled band-like impurity levels. Note in this context however that the very correlation details of *bulk* $\text{SrTiO}_{3-\delta}$ still need to be investigated by similar means

In the higher V_O -concentration regime we focussed on the Ti_3O_5 stoichiometry, studying the metallic Magnéli γ -phase as well as a theory-derived metallic defect-rutile phase. The interplay of Ti coordination and (t_{2g}, e_g) electronic structure properties were discussed and therefrom the differences in total energy and in the spectral features

explained. While $\gamma\text{-Ti}_3\text{O}_5$ turns out as a 'textbook'-like correlated metal, the defect-rutile version displays spectral-weight transfers to higher energies in a much broader (incoherent) fashion. Charge disproportionation is a natural by-product of the V_O ordering in rutile-based TiO_2 (which formally includes the Magnéli phases)¹⁵ and is already captured on the Kohn-Sham level. Electronic correlations beyond the latter provide at least for Ti_3O_5 only minor changes to the Ti charging states.

Although in direct comparison, defect-rutile Ti_3O_5 is energetically rather unfavorable compared to the Magnéli phase, its discussion is nonetheless relevant in view of engineering memristive processes and devices. Since there in TiO_2 , transport of V_O s and electrons when starting from the rutile structure is a possible technological aspect. In fact, in realistic close-to-device-like TiO_2 materials, the formation of defect-rutile *and* Magnéli $\text{Ti}_n\text{O}_{2n-1}$ phases may happen in parallel within a given materials system.⁹ Thus understanding the differences between both structural types on a basic level is of crucial importance. In the long run, the present study shall contribute to pave the road for elucidating further engineering options in the interplay between the transport of oxygen vacancies and electrons.

It would also be highly interesting to extend the present investigation to the rutile VO_2 system. As the vanadium ion in the +4 oxidation state has $3d^1$ occupation, it is known that already the stoichiometric system is prone to strong correlation physics,^{72–76} possibly giving reason to the hallmark metal-to-insulator transition slightly above room temperature.⁷⁷ Recent doping studies of VO_2 via oxygen vacancies display opportunities to tune the competition between the metallic and insulating regime.^{78,79}

Finally coming back to basic features of V_O s in transition-metal oxides, our examination challenges the simplest views on in-gap states, namely the weak-coupling defect-level and the strong-coupling Hubbard-band paradigm. Albeit one encounters features of both original mechanisms in oxygen-deficient TiO_2 , as in related systems such as $\text{SrTiO}_{3-\delta}$ or the $\text{LaAlO}_3/\text{SrTiO}_3$ interface, a unique and well-defined picture describing the general nature of defects in transition-metal oxides is still missing. Crystal-field effects, renormalizations, Hubbard-band formation, lifetime effects, p - d hybridization, screening, charge transfer, polaron formation, etc. are potentially part of this demanding physics. Thoughts trying to put the problem in an adequate model setting have been put forward from several perspectives, e.g. Ref. 80. The future task is to cast those into a sound and solid materials-dependent picture.

ACKNOWLEDGMENTS

We gratefully acknowledge financial support from the German Science Foundation (DFG) via SFB986 and through FOR1346. Computations were performed at the University of Hamburg and the JURECA Cluster of the

- ¹ W. Luo, W. Duan, S. G. Louie, and M. L. Cohen, Phys. Rev. B **70**, 214109 (2004).
- ² N. Pavlenko, T. Kopp, E. Y. Tsymbal, J. Mannhart, and G. A. Sawatzky, Phys. Rev. B **86**, 064431 (2012).
- ³ C. Mitra, C. Lin, J. Robertson, and A. A. Demkov, Phys. Rev. B **86**, 155105 (2012).
- ⁴ J. Shen, H. Lee, R. Valentí, and H. O. Jeschke, Phys. Rev. B **86**, 195119 (2012).
- ⁵ F. Lechermann, L. Boehnke, D. Grieger, and C. Piefke, Phys. Rev. B **90**, 085125 (2014).
- ⁶ F. Lechermann, H. O. Jeschke, A. J. Kim, S. Backes, and R. Valentí, Phys. Rev. B **93**, 121103(R) (2016).
- ⁷ M. Altmeyer, H. O. Jeschke, O. Hijano-Cubelos, C. Martins, F. Lechermann, K. Koepnik, A. Santander-Syro, M. J. Rozenberg, R. Valentí, and M. Gabay, Phys. Rev. Lett. **116**, 157203 (2016).
- ⁸ J. J. Yang, D. B. Strukov, and D. R. Stewart, Nat. Nanotechnol. **8**, 13 (2013).
- ⁹ D.-H. Kwon, K. M. Kim, J. H. Jang, J. M. Jeon, M. H. Lee, G. H. Kim, X.-S. Li, G.-S. Park, B. Lee, S. Han, et al., Nat. Nanotechnol. **5**, 148 (2010).
- ¹⁰ W. Heckel, M. Wehlau, S. B. Maisel, T. Frauenheim, J. M. Knaup, and S. Müller, Phys. Rev. B **92**, 214104 (2015).
- ¹¹ M. Behrmann and F. Lechermann, Phys. Rev. B **92**, 125148 (2015).
- ¹² S. Åsbrink and A. Magnéli, Acta Cryst. **12**, 575 (1959).
- ¹³ S. Andersson and L. Jahnberg, Ark. Kemi **21**, 413 (1963).
- ¹⁴ L. A. Bursill and B. G. Hyde, Prog. Solid State Chem. **7**, 177 (1972).
- ¹⁵ L. Liborio and N. Harrison, Phys. Rev. B **77**, 104104 (2008).
- ¹⁶ A. Janotti, J. B. Varley, P. Rinke, N. Umezawa, G. Kresse, and C. G. V. de Walle, Phys. Rev. B **81**, 085212 (2010).
- ¹⁷ P. Deák, B. Aradi, and T. Frauenheim, Phys. Rev. B **86**, 195206 (2012).
- ¹⁸ A. Janotti, C. Franchini, J. B. Varley, G. Kresse, and C. G. V. de Walle, Phys. Status Solidi RRL **7**, 199 (2013).
- ¹⁹ D. Berger, H. Oberhofer, and K. Reuter, Phys. Rev. B **92**, 075308 (2015).
- ²⁰ G. C. Vásquez, S. Z. Karazhanov, D. Maestre, A. Cremades, J. Piqueras, and S. E. Foss, Phys. Rev. B **94**, 235209 (2016).
- ²¹ G. Mattioli, F. Filippone, P. Alippi, and A. A. Bonapasta, Phys. Rev. B **78**, 241201(R) (2008).
- ²² G. Mattioli, P. Alippi, F. Filippone, R. Caminiti, and A. A. Bonapasta, J. Phys. Chem. C **114**, 21694 (2010).
- ²³ B. J. Morgan and G. W. Watson, J. Phys. Chem. C **114**, 2321 (2010).
- ²⁴ C. Lin, D. Shin, and A. A. Demkov, J. Appl. Phys. **117**, 225703 (2015).
- ²⁵ I. Leonov, A. N. Yaresko, V. N. Antonov, U. Schwingenschlögl, V. Eyert, and V. I. Anisimov, J. Phys.: Condens. Matter **18**, 10955 (2006).
- ²⁶ A. Padilha, J. M. Osorio-Guillén, A. R. Rocha, and G. M. Dalpian, Phys. Rev. B **90**, 035213 (2014).
- ²⁷ K. Tanaka, T. Nasu, Y. Miyamoto, N. Ozaki, S. Tanaka, T. Nagata, F. Hakoe, M. Yoshikiyo, K. Nakagawa, Y. Umeta, et al., Cryst. Growth Des. **15**, 653 (2015).
- ²⁸ D. A. H. Hanaor and C. C. Sorrell, J. Mater. Sci. **46**, 855 (2011).
- ²⁹ J. P. Perdew, A. Ruzsinszky, G. I. Csonka, O. A. Vydrov, G. E. Scuseria, L. A. Constantin, X. Zhou, and K. Burke, Phys. Rev. Lett. **100**, 136406 (2008).
- ³⁰ G. Kresse and J. Hafner, Phys. Rev. B **47**, 558 (1993).
- ³¹ G. Kresse and J. Hafner, Phys. Rev. B **49**, 14251 (1994).
- ³² G. Kresse and J. Furthmüller, Phys. Rev. B **54**, 11169 (1996).
- ³³ G. Kresse and J. Furthmüller, Computational Materials Science **6**, 15 (1996).
- ³⁴ S. Y. Savrasov, G. Kotliar, and E. Abrahams, Nature **410**, 793 (2001).
- ³⁵ L. V. Pourovskii, B. Amadon, S. Biermann, and A. Georges, Phys. Rev. B **76**, 235101 (2007).
- ³⁶ D. Grieger, C. Piefke, O. E. Peil, and F. Lechermann, Phys. Rev. B **86**, 155121 (2012).
- ³⁷ S. G. Louie, K. M. Ho, and M. L. Cohen, Phys. Rev. B **19**, 1774 (1979).
- ³⁸ B. Meyer, C. Elsässer, F. Lechermann, and M. Fähnle, *Fortran 90 program for mixed-basis-pseudopotential calculations for crystals*.
- ³⁹ A. N. Rubtsov, V. V. Savkin, and A. I. Lichtenstein, Phys. Rev. B **72**, 035122 (2005).
- ⁴⁰ P. Werner, A. Comanac, L. de' Medici, M. Troyer, and A. J. Millis, Phys. Rev. Lett. **97**, 076405 (2006).
- ⁴¹ O. Parcollet, M. Ferrero, T. Ayral, H. Hafermann, I. Krivenko, L. Messio, and P. Seth, Comput. Phys. Commun. **196**, 398 (2015).
- ⁴² P. Seth, I. Krivenko, M. Ferrero, and O. Parcollet, Comput. Phys. Commun. **200**, 274 (2016).
- ⁴³ J. P. Perdew, K. Burke, and M. Ernzerhof, Phys. Rev. Lett. **77**, 3865 (1996).
- ⁴⁴ B. Amadon, F. Lechermann, A. Georges, F. Jollet, T. O. Wehling, and A. I. Lichtenstein, Phys. Rev. B **77**, 205112 (2008).
- ⁴⁵ V. I. Anisimov, D. E. Kondakov, A. V. Kozhevnikov, I. A. Nekrasov, Z. V. Pchelkina, J. W. Allen, S.-K. Mo, H.-D. Kim, P. Metcalf, S. Suga, et al., Phys. Rev. B **71**, 125119 (2005).
- ⁴⁶ M. Aichhorn, L. Pourovskii, V. Vildosola, M. Ferrero, O. Parcollet, T. Miyake, A. Georges, and S. Biermann, Phys. Rev. B **80**, 085101 (2009).
- ⁴⁷ K. Haule, C.-H. Yee, and K. Kim, Phys. Rev. B **81**, 195107 (2010).
- ⁴⁸ M. Karolak, T. O. Wehling, F. Lechermann, and A. I. Lichtenstein, J. Phys.: Condens. Matter **23**, 085601 (2011).
- ⁴⁹ T. Mizokawa and A. Fujimori, Phys. Rev. B **51**, 12880R (1995).
- ⁵⁰ E. Pavarini, S. Biermann, A. Poteryaev, A. I. Lichtenstein, A. Georges, and O. K. Andersen, Phys. Rev. Lett. **92**, 176403 (2004).
- ⁵¹ S. Okamoto, A. J. Millis, and N. A. Spaldin, Phys. Rev. Lett. **97**, 056802 (2006).
- ⁵² F. Lechermann and M. Obermeyer, New J. Phys. **17**, 043026 (2015).
- ⁵³ V. I. Anisimov, I. V. Solov'yev, M. A. Korotin, M. T.

- Czyżyk, and G. A. Sawatzky, *Phys. Rev. B* **48**, 16929 (1993).
- ⁵⁴ J. K. Burdett, T. Hughbanks, G. J. Miller, J. W. Richardson Jr., and J. V. Smith, *J. Am. Chem. Soc.* **109**, 3639 (1987).
- ⁵⁵ D. C. Cronmeyer and M. A. Gilleo, *Phys. Rev.* **82**, 975 (1951).
- ⁵⁶ D. C. Cronmeyer, *Phys. Rev.* **87**, 876 (1952).
- ⁵⁷ J. Pascual, J. Camassel, and H. Mathieu, *Phys. Rev. B* **18**, 5606 (1978).
- ⁵⁸ J. C. Parker and R. W. Siegel, *Appl. Phys. Lett.* **57**, 943 (1990).
- ⁵⁹ A. G. Thomas, W. R. Flavell, A. K. Mallick, A. R. Kumarasinghe, D. Tsoutsou, N. Khan, C. Chatwin, S. Rayner, G. C. Smith, R. L. Stockbauer, et al., *Phys. Rev. B* **75**, 035105 (2007).
- ⁶⁰ S. Wendt, P. T. Sprunger, E. Lira, G. K. H. Madsen, Z. Li, J. Ø. Hansen, J. Matthiesen, A. Blekinge-Rasmussen, E. Lægsgaard, B. Hammer, et al., *Science* **320**, 1755 (2008).
- ⁶¹ C. M. Yim, C. L. Pang, and G. Thornton, *Phys. Rev. Lett.* **104**, 036806 (2010).
- ⁶² T. C. Rödel, F. Fortuna, F. Bertran, M. Gabay, M. J. Rozenberg, A. F. Santander-Syro, , and P. Le Fèvre, *Phys. Rev. B* **92**, 041106(R) (2015).
- ⁶³ M. Setvin, C. Franchini, X. Hao, M. Schmid, A. Janotti, M. Kaltak, C. G. V. de Walle, G. Kresse, and U. Diebold, *Phys. Rev. Lett.* **113**, 086402 (2014).
- ⁶⁴ E. Yagi, R. R. Hasiguti, and M. Aono, *Phys. Rev. B* **54**, 7945 (1996).
- ⁶⁵ S. Yang, L. E. Halliburton, A. Manivannan, P. H. Bunton, D. B. Baker, M. Klemm, S. Horn, and A. Fujishima, *Appl. Phys. Lett.* **94**, 162114 (2009).
- ⁶⁶ S.-H. Hong and S. Åsbrink, *Acta Cryst. B* **38**, 2570 (1982).
- ⁶⁷ M. Onoda, *J. Sol. State Chem.* **136**, 67 (1998).
- ⁶⁸ S. Ohkoshi, Y. Tsunobuchi, T. Matsuda, K. Hashimoto, A. Namai, F. Hakoe, and H. Tokoro, *Nat. Chem.* **2**, 539 (2010).
- ⁶⁹ K. Kobayashi, M. Taguchi, M. Kobata, K. Tanaka, H. Tokoro, H. Daimon, T. Okane, H. Yamagami, E. Ikenaga, and S. Ohkoshi, *Phys. Rev. B* **95**, 085133 (2017).
- ⁷⁰ Y. Ishida, R. Eguchi, M. Matsunami, K. Horiba, M. Taguchi, A. Chainani, Y. Senba, H. Ohashi, H. Ohta, and S. Shin, *Phys. Rev. Lett.* **100**, 056401 (2008).
- ⁷¹ L. Boehnke, F. Nilsson, F. Aryasetiawan, and P. Werner, *Phys. Rev. B* **94**, 201106(R) (2016).
- ⁷² A. Zylbersztejn and N. Mott, *Phys. Rev. B* **11**, 4383 (1975).
- ⁷³ C. Sommers and S. Doniach, *Solid State Commun.* **28**, 133 (1978).
- ⁷⁴ T. M. Rice, H. Launois, and J. P. Pouget, *Phys. Rev. Lett.* **73**, 3042 (1994).
- ⁷⁵ S. Biermann, A. Poteryaev, A. I. Lichtenstein, and A. Georges, *Phys. Rev. Lett.* **94**, 026404 (2005).
- ⁷⁶ O. Nájera, M. Civelli, V. Dobrosavljević, and M. J. Rozenberg, *Phys. Rev. B* **95**, 035113 (2017).
- ⁷⁷ F. J. Morin, *Phys. Rev. Lett.* **3**, 34 (1959).
- ⁷⁸ J. Jeong, N. Aetukuri, T. Graf, T. D. Schladt, M. G. Samant, and S. S. P. Parkin, *Science* **339**, 1402 (2013).
- ⁷⁹ Z. Zhang, F. Zuo, C. Wan, A. Dutta, J. Kim, J. Rensberg, R. Nawrodt, H. Hejin Park, T. J. Larrabee, X. Guan, et al., *Phys. Rev. Applied* **7**, 034008 (2017).
- ⁸⁰ F. D. M. Haldane and P. W. Anderson, *Phys. Rev. B* **13**, 2553 (1976).